Received: 11 October 2022 | Revised: 19 February 2024 | Accepted: 20 February 2024

DOI: 10.1111/jnc.16091

Journal of Neurochemistry JNC The Official Journal of the International Society for Neurochemistry WILEY

ORIGINAL ARTICLE

Metabolic response of auditory brainstem neurons to their broad physiological activity range

Nicola Palandt[1,2] | Cibell Resch[1] | Patricia Unterlechner[1] | Lukas Voshagen[1] | Valentin R. Winhart[1,2] | Lars Kunz[1]

[1]Division of Neurobiology, Faculty of Biology, Ludwig-Maximillians-Universität (LMU), Munich, Germany

[2]Graduate School of Systemic Neurosciences (GSN), Ludwig-Maximillians-Universität (LMU), Munich, Germany

Correspondence
Lars Kunz, Division of Neurobiology, Faculty of Biology, Ludwig-Maximilians-Universität München, Grosshaderner Str. 2, D-82152 Planegg, Germany.
Email: lars.kunz@bio.lmu.de

Funding information
Deutsche Forschungsgemeinschaft, Grant/Award Number: DFG KU 1282/9-1

Abstract

Neurons exhibit a high energetic need, and the question arises as how they metabolically adapt to changing activity states. This is relevant for interpreting functional neuroimaging in different brain areas. Particularly, neurons with a broad firing range might exhibit metabolic adaptations. Therefore, we studied MNTB (medial nucleus of the trapezoid body) principal neurons, which generate action potentials (APs) at frequencies up to several hundred hertz. We performed the experiments in acute brainstem slices of the Mongolian gerbil (*Meriones unguiculatus*) at 22.5–24.5°C. Upon electrical stimulation of afferent MNTB fibres with 400 stimuli at varying frequencies, we monitored autofluorescence levels of NAD(P)H and FAD and determined the extremum amplitudes of their biphasic response. Additionally, we compared these data with alterations in O_2 concentrations measured with an electrochemical sensor. These O_2 changes are prominent since MNTB neurons rely on oxidative phosphorylation as shown by our pharmacological experiments. We calculated the O_2 consumption rate as change in O_2 concentration divided by stimulus durations, because these periods varied inversely with stimulus frequency as a result of the constant number of 400 stimuli applied. The O_2 consumption rate increased with stimulation frequency up to a constant value at 600 Hz; that is, energy demand depends on temporal characteristics of activity despite the same number of stimuli. The rates showed no correlation with peak amplitudes of NAD(P)H or FAD, whilst the values of the two molecules were linearly correlated. This points at the complexity of analysing autofluorescence imaging for quantitative metabolic studies, because these values report only relative net changes of many superimposed oxidative and reductive processes. Monitoring O_2 concentration rates is, thus, an important tool to improve the interpretation of NAD(P)H/FAD autofluorescence data, as they do not under all conditions and in all systems appropriately reflect the metabolic activity or energy demand.

Abbreviations: ACSF, artificial cerebrospinal fluid; AP, action potential; ATP, adenosine triphosphate; FAD, oxidised form of flavin adenine dinucleotide; $FADH_2$, reduced form of flavin adenine dinucleotide; LSO, lateral superior olive; MNTB, medial nucleus of the trapezoid body; NADH, reduced form of nicotinamide adenine dinucleotide; NADPH, reduced form of nicotinamide adenine dinucleotide phosphate; OxPhos, oxidative phosphorylation; ROI, region of interest; SEM, standard error of mean; SOC, superior olivary complex; TCA, tricarboxylic acid cycle.

This article is part of the special issue "14th International Conference on Brain Energy Metabolism: Energy Substrates and Microbiome Govern Brain Bioenergetics and Cognitive Function with Aging".

KEYWORDS
autofluorescence, FAD, MNTB, NADH, neuroenergetics, O_2

1 | INTRODUCTION

The brain consumes a major fraction of the body's energy, even though it accounts for only 2% of the human body weight (Camandola & Mattson, 2017; Mink et al., 1981). Energy in form of adenosine triphosphate (ATP) is crucial for neurons to perform their electrical tasks and to sustain housekeeping processes (Howarth et al., 2012). Dysfunctions in neuronal metabolism can contribute to neurodegenerative disorders such as Alzheimer's or Parkinson's disease (Butterfield & Halliwell, 2019; Koopman et al., 2013; Lin & Beal, 2006; Schon & Przedborski, 2011; Watts et al., 2018) and can cause damage after seizures or traumatic brain injuries (Karelina & Weil, 2016; Stovell et al., 2018; Zsurka & Kunz, 2015). Furthermore, neuronal metabolism represents the base for non-invasive functional neuroimaging (Raichle & Mintun, 2006; Shulman et al., 2014). Therefore, understanding the relationship of neuronal activity and metabolism is a prerequisite for analysing neuroimaging data (Raichle & Mintun, 2006; Shulman et al., 2014). The principles of this relationship are important, since neuronal activity patterns, energy consumption and the correlation between them can vary substantially between different brain regions (Sokoloff, 1981). Changes in brain activity were shown to result in alteration of cellular metabolism (Dienel & Cruz, 2016; Zuend et al., 2020).

We were interested whether neurons with a broad activity range would adapt their metabolism to changes in firing frequency. Such an adaptation might represent a kind of optimisation of the energy supply dependent on the activity state. Energy-efficient optimisation was shown on different levels in neurons, for instance for action potential (AP) generation (Alle et al., 2009; Hallermann et al., 2012). So far, only a few studies compared different stimulation frequencies and regimes to study potential adaptation of metabolism to neuronal activity (Brennan et al., 2006; Brosel et al., 2018; Galeffi et al., 2011; Ivanov et al., 2014; Ivanov & Zilberter, 2011; Özugur et al., 2020). We studied the medial nucleus of the trapezoid body (MNTB) in acute brainstem slices of the Mongolian gerbil (*Meriones unguiculatus*; Figure 1). The MNTB is part of the superior olivary complex (SOC), which is contributing to sound source localisation (Grothe et al., 2010). Its principal neurons represent the only neuron type in the MNTB and are functionally well-described (Borst & van Hoeve, 2012; von Gersdorff & Borst, 2002). They are capable of generating synaptically driven APs with frequencies of up to 1000 Hz (Kopp-Scheinpflug et al., 2003; Taschenberger & von Gersdorff, 2000) and exhibit a very low membrane resistance allowing for extraordinary temporal precision (Borst & van Hoeve, 2012; von Gersdorff & Borst, 2002). MNTB neurons become less reliable at stimulation frequencies above 300 Hz; that is, because of synaptic failures, not every individual pre-synaptic stimulus will elicit a post-synaptic AP (Kopp-Scheinpflug et al., 2003). It was suggested that biophysical specialities of MNTB neurons might be the reason for the high energy demand of the MNTB reported by Sokoloff (Sokoloff, 1981). Several studies provided further evidence for this assumption and showed that the MNTB represents a relevant model for neuroenergetics (Lucas et al., 2018; Lujan et al., 2016, 2021; Trattner et al., 2013).

We addressed the question of metabolic alterations related to different firing frequencies by monitoring autofluorescence intensity of the reduced forms of nicotinamide adenine dinucleotide (NADH) and nicotinamide adenine dinucleotide phosphate (NADPH) and of the oxidised form of flavin adenine dinucleotide (FAD) as important molecules in metabolic pathways. A major advantage of this autofluorescence approach is its independence of an uptake of a sensor molecule and the possibility to record simultaneously from a large neuron population. Throughout the manuscript, we will use the term NAD(P)H when talking about imaging data, because NADH and NADPH can normally not be distinguished in autofluorescence imaging. However, only NADH levels change quickly upon energy consumption by AP generation (Shuttleworth, 2010). Both, $FADH_2$ (reduced form of flavin adenine dinucleotide) and NADH are oxidised in the electron transport chain in the mitochondria to produce ATP during oxidative phosphorylation (OxPhos). This process is accompanied by a reduction of O_2 to water. Therefore, we additionally monitored juxta-cellular O_2 concentrations with an electrochemical sensor at the site of NAD(P)H/FAD imaging (Brosel et al., 2018; Huchzermeyer et al., 2013). NADH and $FADH_2$ are regenerated by reduction in the tricarboxylic acid (TCA) cycle and for NADH in several additional metabolic pathways (e.g. glycolysis). The majority of the NAD(P)H autofluorescence originates from mitochondria, because of an increased fluorescence lifetime of protein-bound NAD(P)H in this organelle (Schaefer et al., 2019; Shuttleworth, 2010). Therefore, we detected mainly changes in NADH levels during TCA cycle activity and OxPhos, similar to the FAD levels. The measured autofluorescence levels of NAD(P)H and FAD reflect the net balance of all their oxidative and reductive processes. Upon stimulation, the rapid oxidisation of NADH/$FADH_2$ sets in, followed by their reduction (Schaefer et al., 2019; Shuttleworth, 2010) resulting in a net biphasic response with a NAD(P)H dip and a FAD peak. However, as the biphasic response is the result of the complex superposition of different reduction and oxidation processes, we compared the net peak/dip amplitudes with O_2 level changes as quantitative measure for oxidative processes. In the lateral superior olive (LSO), an auditory brainstem nucleus with biophysical similarities to the MNTB, we found a non-linear response of changes in NAD(P)H and FAD levels with increasing stimulation frequency. Therefore, we were interested whether such a frequency dependency is a general feature in auditory nuclei with specialised neurons. We stimulated MNTB neurons via their afferent fibres and applied different stimulation

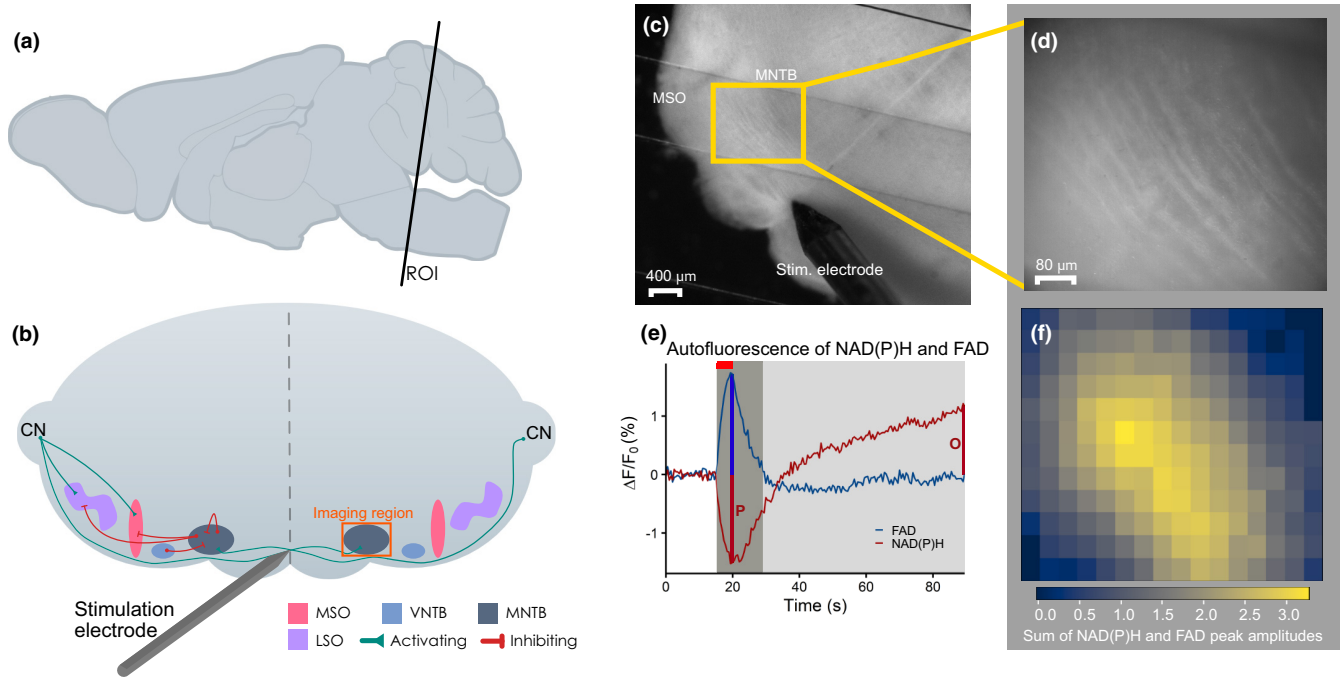

FIGURE 1 Monitoring of NAD(P)H and FAD autofluorescence in the MNTB during neuronal activity. (a) Schematic of the brain of a Mongolian gerbil in lateral view. The black line represents the position of the acute slices used. ROI, region of interest. (b) Brainstem slice with the MNTB, other SOC nuclei and major connections between the nuclei. The concentric bipolar stimulation electrode is placed at the midline to activate the fibres of the globular bushy cells leading to the MNTB. MNTB, medial nucleus of the trapezius body; MSO, medial superior olive; LSO, lateral superior olive; VNTB, ventral nucleus of the trapezius body; CN, cochlear nucleus. (c, d) Bright-field images of an acute auditory brainstem slice with a stimulation (Stim.) electrode placed in the midline. Image at 5× magnification with MNTB, MSO and LSO (c) and at 20× magnification showing the MNTB (d; magnification of area in rectangle in (c)). (e) Time course of a typical NAD(P)H and FAD autofluorescence recording with electrical stimulation for 5 s (at 5 V/200 Hz shown as red horizontal line). The net oxidative phase is labelled as dark grey area, the net NAD(P)H reductive phase in light grey. FAD peak amplitude is depicted as vertical blue line, NAD(P)H peak amplitude as red line labelled with 'P' and NAD(P)H overshoot as red line with the label 'O'. Note that in the initial components of the net oxidative phase (starting at stimulus onset) from baseline to the peaks (to the left of the red/blue lines), oxidation greatly exceeds reduction, whereas after attaining the peak values, reduction exceeds oxidation and the fluorescence values return towards baseline (to the right of the red/blue lines). (f) The heatmap (same region as in (d)) shows for each ROI the sum of the peak amplitudes of NAD(P)H and FAD autofluorescence. FAD, oxidised form of flavin adenine dinucleotide; NAD(P)H, reduced form of nicotinamide adenine dinucleotide and nicotinamide adenine dinucleotide phosphate.

protocols (continuous stimulation duration, fixed number of stimuli and burst-like stimuli), since theoretical considerations predicted a stronger influence of firing rate than of firing pattern to neuronal energy demand (Yi & Grill, 2019).

Glucose concentrations in experimental studies differ substantially. In most electrophysiological in vitro studies using brain slices, a glucose concentration of 10 or even 25 mM was utilised (Hollnagel et al., 2020; Lourenço et al., 2019). In our metabolic LSO study (Brosel et al., 2018), we used only 2 mM glucose, which corresponds to the physiological glucose concentration in vascularised brain tissue. However, this has to be seen under the assumption that diffusion in the slice does not limit glucose provision. One major difference between acute slices and the brain in vivo is the missing circulation in slices, in which nutrients (e.g. glucose) and O_2 are provided by diffusion out of the bath solution. Only a few studies have addressed this issue so far and studied the impact of varying concentrations of glucose and/or O_2 (Foster et al., 2005; Galeffi et al., 2011; Huchzermeyer et al., 2008; Ivanov et al., 2014; Ivanov & Zilberter, 2011; Özugur et al., 2020; Sünwoldt et al., 2017). We, therefore, compared measurements with 2 and 10 mM glucose in the MNTB.

2 | MATERIALS AND METHODS

2.1 | Animals

The experiments complied with regional regulations (District Government of Upper Bavaria, 'Regierung von Oberbayern'), national laws (§4 of the German Animal Welfare Act; no ethics approval number allocated) and with the European Communities Council Directive (2010/63/EU). Mongolian gerbils (*Meriones unguiculatus*) of either sex bred in our certified in-house breeding facility (German Animal Welfare Act, 4.3.2–5682/ Ludwig-Maximillians-Universität (LMU) Munich /Faculty of Biology) were used for the experiments. Groups of 3 to 4 gerbils were housed in Makrolon™ cages (Typ IV 2000P; Tecniplast; ground area, 2065 cm^2; height, 256 mm with 12 h light/dark cycles at 22.4°C and 66% humidity). We used a total

number of 26 animals (5 animals for every different experiment, 6 animals for the experiment with increased glucose concentration) with an age range between post-natal day 30 and 40 (P30-P40).

2.2 | Brain slice preparation

The animals were anaesthetised with isoflurane and then decapitated. The brain was removed and transferred to ice-cold slicing solution. The slicing solution contained (in mM) 143 sucrose, 25 NaCl, 2.5 KCl, 4 $MgCl_2$, 0.1 $CaCl_2$, 1.25 NaH_2PO_4, 25 $NaHCO_3$, 2 glucose, 3 myo-inositol, 2 pyruvic acid and 0.4 ascorbic acid (Sigma-Aldrich). To adjust a pH of 7.4, the solution was aerated with carbogen (95% O_2, 5% CO_2). Using a VT1200S Vibratome (Leica Microsystems GmbH, Wetzlar, Germany), we cut six 200 μm thick transverse slices enclosing the MNTB. Slices were incubated for 15 min at 36°C in artificial cerebrospinal fluid (ACSF) solution containing (in mM): 23 sucrose, 125 NaCl, 2.5 KCl, 1 $MgCl_2$, 2 $CaCl_2$, 1.25 NaH_2PO_4, 25 $NaHCO_3$ and 2 glucose (Sigma-Aldrich; Brosel et al., 2018). A pH of 7.4 was adjusted by aeration with carbogen. Thereafter, slices were kept at room temperature (23.5°C ± 1°C). The time from decapitation to the start of slice incubation was approximately 15–20 min. The time interval between cutting of first and last slice was 15–20 min.

2.3 | Autofluorescence imaging

Slices were submerged in a recording chamber and constantly superfused with ACSF on the top face. We performed all measurements at room temperature (23.5°C ± 1°C) for a maximum of 5 h after death. The recording chamber is part of our imaging system, which was in detail described by Direnberger et al. (2015). NAD(P)H and FAD were excited with light-emitting diodes (LEDs) at 365 and 470 nm, respectively (Brosel et al., 2018; Huchzermeyer et al., 2008; Schaefer et al., 2019; Shuttleworth, 2010), through a tube lens (425308) and a 20×/1.0 W Plan-Apochromat water-dipping objective (Carl Zeiss Microscopy, Göttingen, Germany). A program using LabVIEW 8.0 (National Instruments, Austin, TX, USA) controlled the objective's z-motion. We recorded the NAD(P)H and the FAD fluorescence images with a camera equipped with a metal–oxide–semiconductor sensor (pco.edge 5.5; PCO AG, Kelheim, Germany) alternatingly every 250 ms with an acquisition time of 20 ms. Fluorescence signals were recorded from the top layer (50–100 μm) of the slice. The illumination was pulsed to minimise photobleaching in the tissue. TTL pulses controlled by the PATCHMASTER software and produced by an EPC10 amplifier (both HEKA, Multi Channel Systems MCS GmbH, Reutlingen, Germany) triggered LEDs, camera and electrical stimulation. We used a multiband filter for excitation (AHF F69-390) and emission (AHF F72-622; AHF analysentechnik AG, Tübingen, Germany). The autofluorescence was recorded in total for 90 s. After 15 s of the measurement, the axon bundle leading to the MNTB neurons was stimulated with a bipolar tungsten electrode (stimulation amplitude, 5 V; tapered tip concentric microelectrodes, MicroProbes, CEA200) placed at the midline. The stimulation frequency was varying in the range of 10–1000 Hz and either the stimulation duration (Figure 2a) or the total number of stimuli was constant (majority of experiments). In these experiments with 400 stimuli, the duration was between 0.4 and 40 s according to the stimulation frequency (Figure 2b). After a stimulation experiment, we waited for 5 min before the next stimulation to allow metabolic recovery, that is for instance replenishment of tissue levels of O_2 and glucose from the medium after depletion by the stimulation. This process is diffusion-limited as can be deduced from our O_2 measurements (Figure 3a). The series of varying frequencies was randomly chosen in each set of experiments to exclude an impact of the series (Brosel et al., 2018). We captured autofluorescence signals of the entire nucleus. Although, for further analysis, we identified the region, where the sum of the amplitudes of NAD(P)H and FAD extrema was highest (Figure 1c–f; see Section 2.4).

2.4 | Pre-processing and data analysis

Autofluorescence videos were analysed using a self-written Python script, which we will share upon reasonable request. The script divided each image into 192 (16×12) rectangular regions of interest (ROI) with a size of approximately 50×50 μm. The ROI with the largest sum of NAD(P)H and FAD peak amplitude in most experiments of the session was chosen for analysis, because we assumed that this was the region to which most of the excited axons projected (Figure 1f). This ROI was used for all subsequent experiments with different frequencies on the same brainstem slice. To correct the bleaching of the autofluorescence, we fitted a linear function to the data points of the first 15 s before the stimulation. The change in autofluorescence ΔF was calculated as the difference between the measured fluorescence and this linear correction function. The fluorescence signals were presented as $\Delta F/F_0$ with F_0 being the fluorescence at the beginning of the stimulation. From the time course of $\Delta F/F_0$ for the two metabolites, we calculated the amplitudes of the net extrema (Figure 1e). To compare them, we analysed the values of the NAD(P)H dip and refer to them as net peak amplitudes for simplicity. Since we used a multiband filter to monitor NAD(P)H and FAD in the same experiment, FAD got excited at 360 nm as well. Therefore, a bleed-through of FAD fluorescence in the NAD(P)H images occurred. To correct for this bleed-through, we subtracted a calculated FAD autofluorescence image from the NAD(P)H autofluorescence image. Details on the correction can be found in the supplement. This correction causes an underestimation of NAD(P)H as our verification of the calculation showed. However, the correction clearly reduced a much larger overestimation by 99% (compared to an underestimation of 23% without correction). In addition to peak amplitudes, we determined the rise time to the extremum ($t_{20/80}$), which refers to the period when the values rise from 20% to 80% of the extremum amplitude. For NAD(P)H, we tracked the overshoot of the time course after the first recovery difference between baseline and maximal overshoot (Figure 1e).

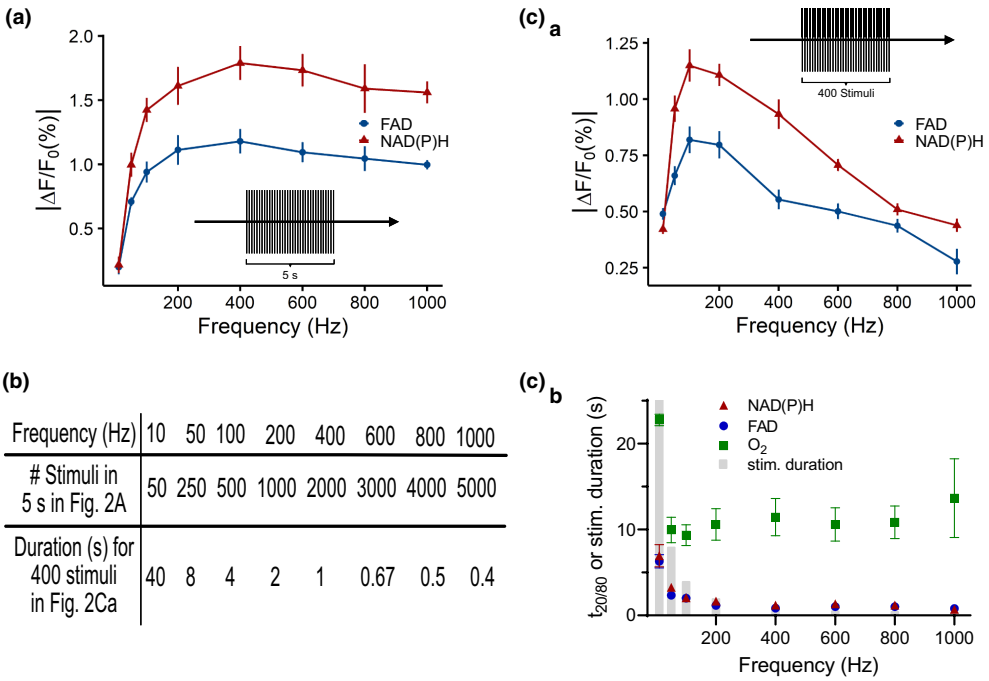

Frequency (Hz)	10	50	100	200	400	600	800	1000
# Stimuli in 5 s in Fig. 2A	50	250	500	1000	2000	3000	4000	5000
Duration (s) for 400 stimuli in Fig. 2Ca	40	8	4	2	1	0.67	0.5	0.4

FIGURE 2 Frequency dependence of NAD(P)H and FAD responses for different stimulation patterns. (a) Peak amplitudes of NAD(P)H and FAD autofluorescence for a 5-s stimulation (inset) at various frequencies and consequently with a differing number of stimuli (see b). (b) Comparison of total number (#) of stimuli for the 5-s stimulation paradigm (data in (a)) and of stimulation duration for experiments applying a fixed number of 400 stimuli (data in (c)). (c) Analysis of NAD(P)H and FAD autofluorescence whilst stimulating MNTB fibres with different frequencies to apply always 400 stimuli (inset) revealing changes in peak amplitudes (Ca) and peak rise time ($t_{20/80}$; Cb). (Cb) Frequency dependence of peak rise time ($t_{20/80}$) of NAD(P)H, FAD (same recordings as in Ca) as well as O_2 concentration (ΔO_2; Figure 3b) after 400 stimuli. The grey bars show the stimulation (stim.) duration in comparison to the rise times (*y*-axis cut at 25 s despite a stim. duration of 40 s for 10 Hz. Data points represent mean +/− SEM; (a), $n = 9$; (c), $n = 10$ independent experiments in 5 brain slices; each from an individual animal. FAD, oxidised form of flavin adenine dinucleotide; NAD(P)H, reduced form of nicotinamide adenine dinucleotide and nicotinamide adenine dinucleotide phosphate.

For FAD, we did not observe any overshoot in the MNTB in contrast to other brain regions (Brosel et al., 2018; Shuttleworth, 2010).

2.5 | Oxygen electrode recordings

Extracellular O_2 was recorded with electrochemical O_2 microelectrodes with a 10 µm-diameter tip (Unisense A/S, Aarhus, Denmark; 90%-response time, 1–3 s; detection limit, 0.3 µM; Brosel et al., 2018; Huchzermeyer et al., 2013). We calibrated the microelectrodes according to the manufacturer's instruction with a 3-point calibration using 0.1 M ascorbic acid in 0.1 M NaOH (0%/0 µM O_2), air-bubbled ACSF (20%/265 µM O_2) and carbogen-bubbled ACSF (95%/1350 µM O_2). The electrode tip was placed exactly at the same level of the slice from which we recorded NAD(P)H and FAD autofluorescence and in the ROI used for analysis, to allow for a correlation of O_2 and NAD(P)H/FAD. The voltage signals of the microelectrode were recorded by means of a microsensor multimeter and the SensorTrace Profiling software (both Unisense). We calculated absolute O_2 concentrations by applying the 3-point calibration in the software. From these absolute values, O_2 level changes (ΔO_2) were calculated as the difference between O_2 concentrations before and at its minimum after stimulation. Using this value, we calculated the O_2 consumption rate as ΔO_2/(stimulus duration) for each individual recording.

2.6 | Pharmacology

To block Complex I, III and IV of the oxidative phosphorylation (OxPhos) we used 10 µM rotenone (Sigma-Aldich; cat. No. 45656 (year 2019); stock solution 5 mM in ethanol), 10 µM antimycin A (Sigma-Aldrich; Cat. No. A8674 (year 2019); stock solution 90 mM in ethanol) and 10 µM potassium cyanide (Sigma-Aldrich; stock solution 10 mM in H_2O). The blockers were added to the ACSF and autofluorescence measurements were taken every 5 min after the start of the washin. After 20 min, the blocker solution was replaced with normal ACSF (washout for 15–20 min). For these measurements, we stimulated the fibres with 50 Hz for 8 s applying 400 APs.

2.7 | Statistical analysis

We have chosen a number of $n = 9$–10 independent experiments based on the minimal number of 5–8 experiments per condition found

in the literature on autofluorescence imaging (Brennan et al., 2006; Foster et al., 2005; Galeffi et al., 2011; Huchzermeyer et al., 2008, 2013; Ivanov et al., 2014; Ivanov & Zilberter, 2011; Liotta et al., 2012) and on our experience in another auditory nucleus (Brosel et al., 2018). In the literature, no sample calculations were found and we have not performed a power calculation. From each individual animal, we used one brain slice for experiments. On each slice, we performed two independent sets of experiments when the tissue showed no detrimental alteration after the first set of stimulations and when the control measurement of the second set entailed similar peak amplitudes. We did not pre-determine any exclusion criteria and did not exclude any data. No randomisation and no blinding was performed in this

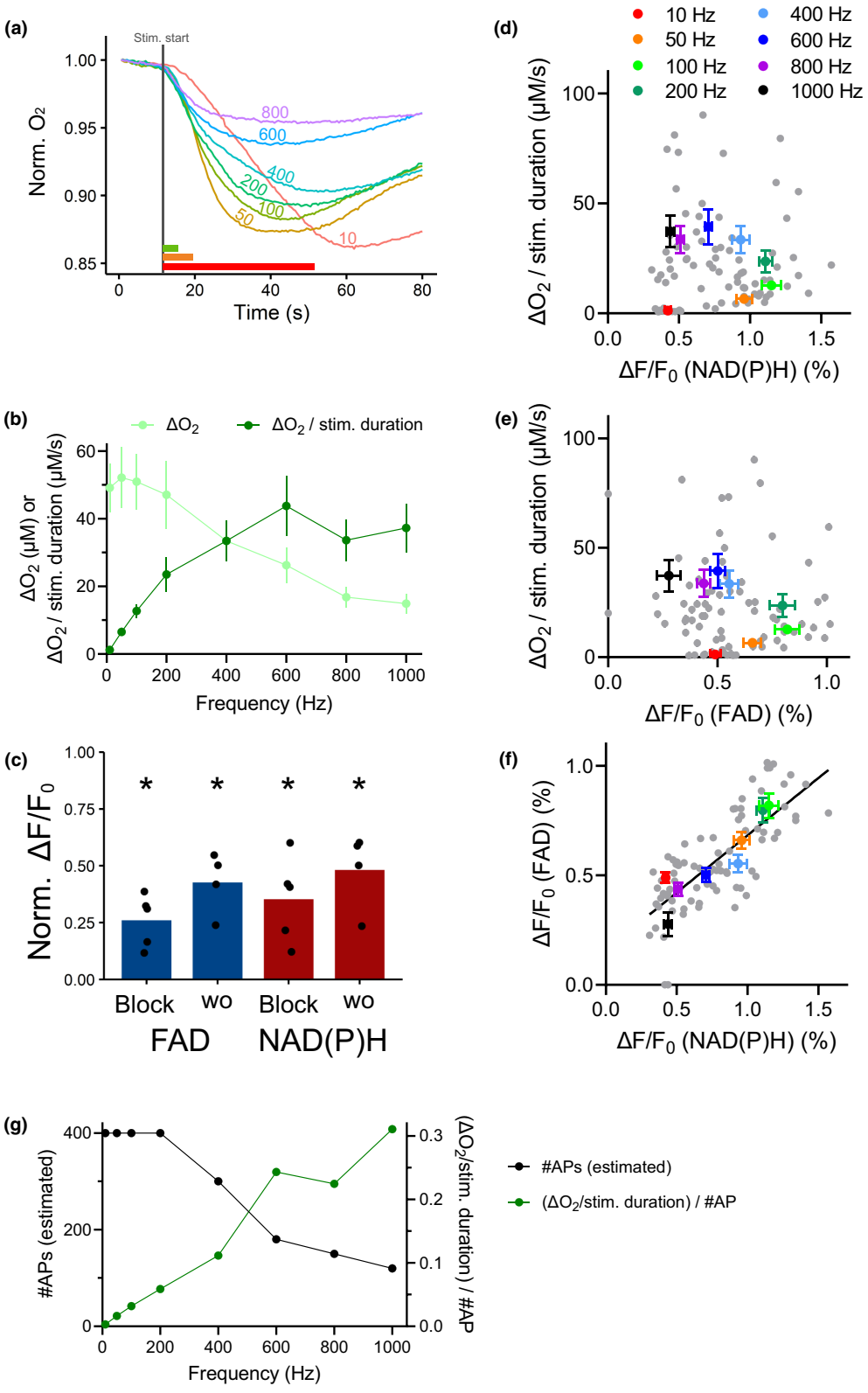

FIGURE 3 Oxygen consumption and role of OxPhos. All data presented in this Figure were obtained by applying a fixed number of 400 stimuli at varying frequencies. (a) Example of time course of the O_2 concentration after stimulation (Stim. start) with different frequencies normalised to the value at the start of the recording ($t = 0$ s). The varying stimulus duration is listed in Figure 2b (bottom row) and depicted as horizontal colour bars in the graph for the three frequencies with the longest duration (10, 50 and 100 Hz). (b) O_2 concentration drop (ΔO_2) and O_2 consumption rate (ΔO_2/stim. duration) for varying stimulation frequencies. ΔO_2 values represent the difference in O_2 concentrations between minimum and start of stimulation. The O_2 consumption rate was calculated by dividing the ΔO_2 values by the varying stimulus (stim.) durations (Figure 2b, bottom row). Depicted are the mean values +/− SEM for the respective frequencies. (c) Pharmacologically blocking of OxPhos with rotenone, antimycin A and potassium cyanide (10 μM each for 20 min; block) in experiments applying 400 stimuli at 50 Hz entailed a pronounced reduction in NAD(P)H and FAD peak amplitudes. The values were normalised to the respective control values before application of blockers. Points represent individual experiments and the bars mean values. All values are significantly different (*) from 1, i.e. the unblocked control condition as tested by one-sample *t*-test (*p* values: NAD(P)H block, 0.0015, df = 4, $t = 7.708$; NAD(P)H wo, 0.0089, df = 3, $t = 6.09$; FAD block, 0.0001, df = 4, $t = 14.47$; FAD wo, 0.0035, df = 3, $t = 8.429$). The washout (wo; 15–20 min) was significantly different from blocking for FAD (paired *t*-test, $p = 0.0070$, df = 4, $t = 6.642$) and showed a tendency for NAD(P)H ($p = 0.0654$, df = 3, $t = 2.844$). (d–f) Correlation between O_2, NAD(P)H and FAD responses. Grey dots represent individual data, whereas coloured dots the mean values (+/− SEM) for the respective frequencies. Linear regression for NAD(P)H vs. FAD peak amplitudes (f) resulted in $p < 0.0001$, $R^2 = 0.563$, df = 78. Data points represent mean +/− SEM; $n = 10$ independent experiments in 5 brain slices; each from an individual animal. (g) Estimation of O_2 consumption rate per AP for a fixed number of 400 stimuli. The graph shows data based on stimulation-induced changes in O_2 consumption rate (ΔO_2/stimulation (stim.) duration; Figure 3b) divided by the estimated number of APs (black dots and line). FAD, oxidised form of flavin adenine dinucleotide; NAD(P)H, reduced form of nicotinamide adenine dinucleotide and nicotinamide adenine dinucleotide phosphate.

study. All data are presented as mean +/− SEM (standard error of the mean). Autofluorescence data (NAD(P)H and FAD) were normalised to baseline before stimulation. In Figure 3c, we normalised the peak amplitudes with pharmacological blockers to the control condition to visualise the effect of inhibiting OxPhos and, therefore, applied a one-sample *t*-test. Statistical analysis was performed in the language package R (www.R-project.org; R Core Team, 2023) or in GraphPad Prism 9.5.1 (GraphPad Software, Boston, MA). Normal distribution of the data was analysed using a Q-Q plot and the Shapiro–Wilk test. We tested statistical significance with a double-sided *t*-test. To test for correlations (Figure 2Cb, 3d–f), we calculated the Pearson correlation coefficient and applied linear regression in some experiments. In all statistical analyses, a *p*-value <0.05 was considered significant. The results of statistical testing can be found in the respective section in Results and in the Figure Legends.

3 | RESULTS

3.1 | Frequency dependence of metabolic responses

In the first set of experiments, we chose a stimulation duration of 5 s according to our previous study in another auditory brainstem nucleus, the lateral superior olive (LSO; Brosel et al., 2018). At low frequencies, the net peak amplitudes of NAD(P)H and FAD rise first from 10 to 400 Hz and then are stable for higher frequencies (Figure 2a) – very similar to recordings in the LSO (Brosel et al., 2018). The rise in net peak amplitudes with increasing stimulation frequency can have two obvious reasons. (1) A direct frequency-dependent process, that is an immediate consequence of the need for more ATP per second because a rising frequency entails more APs per second. (2) A trivial implication of the increased total number of APs because of the constant 5 s stimulation period (from 50 stimuli at 10 Hz to 5000 stimuli at 1000 Hz; Figure 2b, middle row). To identify whether one of these explanations – or both – are valid, we changed the stimulation protocol in such a way that we applied exactly 400 stimuli to the fibre at all frequencies (Figure 2c). Consequently, the stimulation duration varied between 40 s (10 Hz) and 0.4 s (1000 Hz; Figure 2b, bottom row). Similar to the experiments with a constant stimulation period (Figure 2a), at first the net peak amplitudes increase with stimulation frequencies (Figure 2Ca). However, rising the frequency further above 200 Hz resulted in their decrease. As the time course of NAD(P)H and FAD autofluorescence reflects the superposition of various reductive and oxidative processes—with mitochondrial pathways (TCA cycle, OxPhos) being the most visible ones—analysis of other parameters might provide further insights (Brosel et al., 2018). Therefore, we have analysed the peak rise time $t_{20/80}$ that represents the time during which the fluorescence intensity changes from 20% to 80% of the peak amplitude (Figure 2Cb). With increasing stimulation frequency, $t_{20/80}$ was getting shorter and stayed constant for 200 Hz and above. However, at low frequencies the stimulation periods are rather long (grey bars in Figure 2Cb) and for ≤100 Hz even longer than the respective $t_{20/80}$ values. The $t_{20/80}$ values showed a significant correlation with the stimulus duration (NAD(P)H, Pearson correlation coefficient $r = 0.7715$, $p < 0.0001$; NAD(P)H, $r = 0.8678$, $p < 0.0001$; 80 data pairs for both). Therefore, the interpretation is difficult and will be presented in the context of O_2 measurements described in the Section 3.2.

3.2 | Oxygen consumption and contribution of oxidative phosphorylation

In Figure 3a, typical normalised O_2 concentration changes with time are depicted for different stimulation frequencies. At all frequencies, the values continued to decrease after the stimuli ceased and stayed below starting values for durations that greatly exceeded those of the stimuli. In contrast to NAD(P)H/FAD recording, the $t_{20/80}$ values

for O_2 recordings did not depend on stimulus duration and only the 10-Hz values were in their range (Figure 2Cb). Including the 10-Hz values, $t_{20/80}$ for O_2 was significantly correlated with stimulus duration (Pearson correlation coefficient = 0.4692, $p < 0.0001$, 80 data pairs), whilst without them no correlation was observed ($r = -0.1010$; $p = 0.4053$; 70 data pairs). In contrast, $t_{20/80}$ values for NAD(P)H and FAD were significantly correlated also without the 10-Hz values (NAD(P)H, $r = 0.7561$, $p < 0.0001$; FAD, $r = 0.7148$, $p < 0.0001$; 70 data pairs for both). We calculated the stimulation-induced O_2 concentration difference (ΔO_2) and – to account for the varying duration of the electrical stimuli – the O_2 consumption rate (ΔO_2 divided by the stimulus duration; Figure 3b). This rate clearly rose with stimulation frequencies up to 600 Hz and was constant above. We observed a discrepancy between the frequency dependency of autofluorescence imaging (Figure 2Ca) and O_2 recordings. The net peak amplitudes of NAD(P)H and FAD do not show any significant correlation with the O_2 consumption rates (Figure 3d,e; NAD(P)H, Pearson correlation coefficient $r = -0.0028$, $p = 0.980$; FAD: $r = -0.0835$, $p = 0.461$; 80 data pairs for both), whereas the NAD(P)H values are significantly correlated with those for FAD (Figure 3f; $r = 0.7504$, $p < 0.0001$, 80 data pairs).

To show the importance of OxPhos in MNTB principal neurons, we applied 400 fibre stimuli at 50 Hz before and during blockage of OxPhos with rotenone, antimycin A and potassium cyanide (each 10 μM for 20 min). The stimulation-induced net peak amplitudes of both NAD(P)H and FAD were decreased in the presence of the OxPhos inhibitors as can be seen from the values normalised to their respective amplitudes under control conditions (Figure 3c). Washout of the blockers for 15–20 min entailed a significant recovery for FAD and at least a tendency for NAD(P)H peak amplitudes.

3.3 | Estimation of the number of APs at high stimulation frequencies and consequences for the frequency dependency of metabolic responses

At stimulation frequencies above 300 Hz, it is difficult to distinguish between a potential metabolic adaptation and the MNTB principal neurons firing less reliably (see Sections 1, 4 and 4.1). As we have not measured the AP response to different stimulation frequencies, we estimated the number of APs in relation to the number of stimuli based upon in vivo data (Borst & van Hoeve, 2012; Kopp-Scheinpflug et al., 2003, 2011; Taschenberger & von Gersdorff, 2000) and in vitro cell-attached recordings (Grande & Wang, 2011). It is important to determine the failure rate based on these measurements with undisturbed intracellular state. Up to 300 Hz, we equated firing frequency with stimulation frequency. Above this limit, we assumed that the neurons fire on average with only 300 Hz irrespective of the stimulation frequency. Applying this simple assumption, we calculated the estimated number of APs (black dots and lines in Figure 3g). Based on these values, we calculated the O_2 consumption rate (ΔO_2/stimulation duration) per AP, which continuously increased with stimulation frequency (Figure 3g).

3.4 | Burst stimulation

Many neurons, especially those capable of high-frequency firing, are not only continuously active but often show a bursting activity pattern. A computational study has shown that in thalamocortical relay neurons the mean firing rate determines energetic needs more than the temporal firing pattern (Yi & Grill, 2019). To simulate more physiological conditions, we applied 400 stimuli over a constant stimulation period of 5 s for all frequencies (Figure 4a). These 400 stimuli were applied in bursts containing 5 stimuli at the respective stimulation frequency, which are separated from the next burst by breaks with varying duration, dependent on the frequency. Stimulation frequencies below 100 Hz were not applied, because a stimulation period longer than 5 s would have been necessary for 400 stimuli. The changes in NAD(P)H and FAD net peak amplitudes showed no obvious difference to the values for the temporally equally distributed application of 400 stimuli except for the 1000-Hz data (Figure 4b,c; two-sided *t*-test: FAD, $p = 0.024$; NAD(P)H, $p = 0.055$).

3.5 | Glucose dependency of NAD(P)H/FAD responses at different stimulation frequencies

We examined the impact of two different glucose concentrations on the changes in NAD(P)H and FAD amplitudes with 400 stimuli at different frequencies. In all our experiments presented so far, we used solutions with 2 mM glucose like in our study on the LSO (Brosel et al., 2018). In comparison, we applied a solution with 10 mM glucose and no sucrose. The curves exhibit a similar frequency dependency of NAD(P)H and FAD net peak amplitudes (Figure 4d,e). The NAD(P)H net peak amplitudes showed no significant difference, however, the FAD values are significantly smaller for the higher glucose concentration except for 200 Hz and 1000 Hz (double-sided *t*-test, see Figure legend). Amplitudes of the NAD(P)H overshoot are clearly smaller for the higher glucose concentration (Figure 4f; see Figure legend). For FAD autofluorescence, no overshoots were observed at all.

4 | DISCUSSION

4.1 | Experimental approach and its limitations

The advantages of monitoring the autofluorescence of NAD(P)H and FAD are its non-invasive nature, a temporal resolution in the range of seconds and the possibility to record from a large cell population. There has been an extensive discussion on the interpretation of autofluorescence data and the cellular and subcellular origin of the signals. As the major NAD(P)H autofluorescence signal originates from mitochondria because of the increased fluorescence lifetime in this environment, its changes reflect mainly NADH oxidation during OxPhos to regenerate ATP and its reduction in the TCA cycle; just like for FAD, which is not involved in other

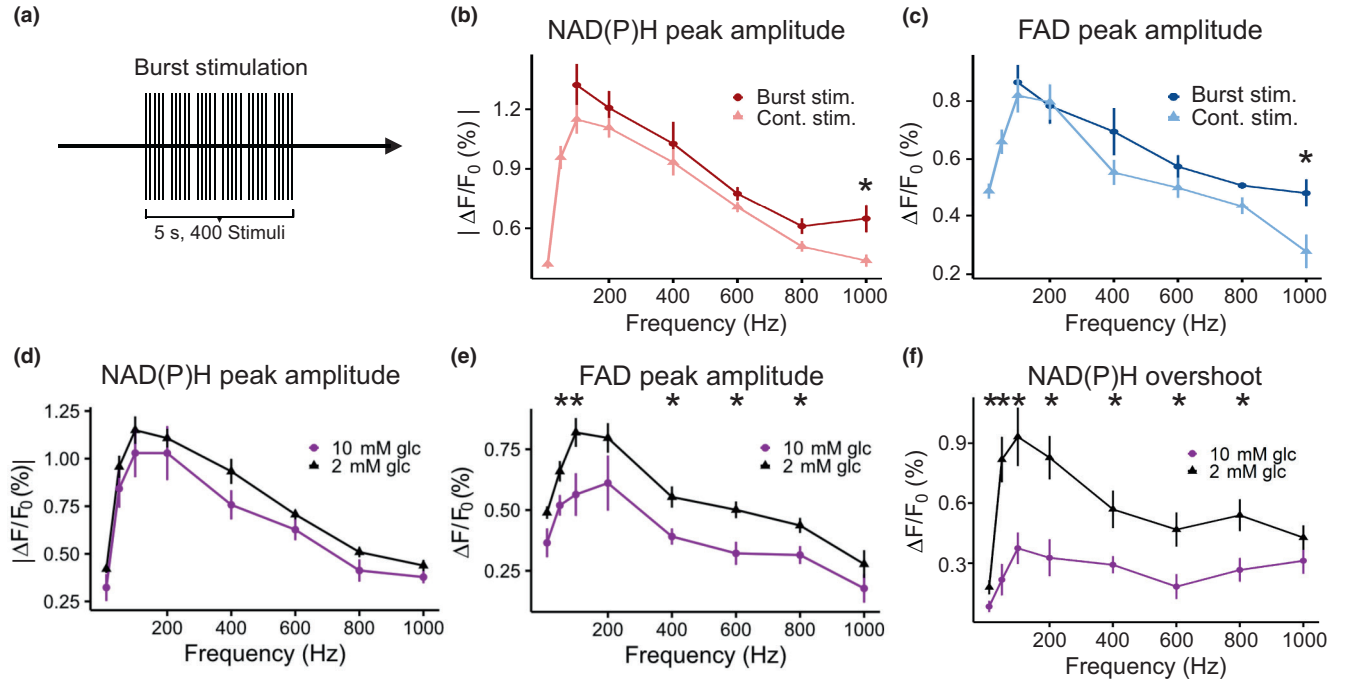

FIGURE 4 Influence of burst mode stimulation and of different glucose (glc) concentrations. (a) Stimulation pattern of burst mode. The 400 stimuli were divided into 80 bursts with 5 stimuli per burst. Consequently, the breaks between two consecutive bursts vary, because the stimulation duration was always 5 s. (b, c) Peak amplitudes of NAD(P)H (b) and FAD (c) for different frequencies in burst mode (Burst stim.). For comparison, we replotted the data for continuous stimulation (Cont. stim.) with 400 stimuli (Figure 2Ca). Only the values at 1000 Hz were significantly different (*; FAD: $p = 0.024$, df = 12.305, $t = 2.573$; NAD(P)H: $p = 0.055$, df = 6.124, $t = 2.367$). Data points (in B, C) represent mean +/− SEM; $n = 7$ independent experiments (600 and 800 Hz, $n = 3$) in 5 brain slices (3 for 600 and 800 Hz); each from an individual animal. (d–f) Frequency dependency of autofluorescence responses at different extracellular glucose (glc) concentrations after 400 stimuli continuously applied. (d, e) Peak amplitudes of NAD(P)H (D) and FAD (E) for a glucose concentration of 2 mM (same data as shown in Figure 2Ca) and 10 mM. NAD(P)H, no significant difference; FAD, 10 Hz, $p = 0.064$, df = 12.264, $t = -2.034$; 50 Hz, $p = 0.028$, df = 16.8, $t = -2.404$; 100 Hz, $p = 0.017$, df = 17.646, $t = -2.626$; 200 Hz, $p = 0.222$, df = 8.434, $t = -1.317$; 400 Hz, $p = 0.006$, df = 16.813, $t = -3.129$; 600 Hz, $p = 0.007$, df = 14.489, $t = -3.117$; 800 Hz, $p = 0.019$, df = 15.832, $t = -2.6$; 1000 Hz, $p = 0.228$, df = 16.686, $t = -1.25$; double-sided *t*-test; *$p < 0.05$. (f) Analysis of the overshoot of the NAD(P)H time course (double-sided *t*-test; *$p < 0.05$: 10 Hz, $p = 0.043$, df = 16.69, $t = -2.18$; 50 Hz, $p = 0.0004$, df = 16.015, $t = -4.5$; 100 Hz, $p = 0.003$, df = 13.503, $t = -3.57$; 200 Hz, $p = 0.003$, df = 15.903, $t = -3.532$; 400 Hz, $p = 0.015$, df = 12.908, $t = -2.807$; 600 Hz, $p = 0.013$, df = 16.341, $t = -2.8$; 800 Hz, $p = 0.011$, df = 16.442, $t = -2.866$; 1000 Hz, $p = 0.200$, df = 16.385, $t = -1.317$). Data points (in d–f) represent mean ±SEM; $n = 10$ (2 mM glc) and $n = 9$ independent experiments (10 mM glc), respectively in 6 brain slices (5 for 2 mM glc); each from an individual animal. FAD, oxidised form of flavin adenine dinucleotide; NAD(P)H, reduced form of nicotinamide adenine dinucleotide and nicotinamide adenine dinucleotide phosphate.

cytoplasmic processes (Schaefer et al., 2019; Shuttleworth, 2010). Therefore, the peak amplitudes of NAD(P)H/FAD are often quantified as a measure of ATP generation (Shuttleworth, 2010). However, many metabolic processes determine the intracellular levels of NAD(P)H and FAD, and at equilibrium state, which relates to baseline measurements before stimulation, the net reaction of oxidation and reduction is zero. As the involved metabolic processes can vary with respect to their amplitude and timing, the peak amplitudes might be substantially affected and, thus, do not necessarily reflect the amount of ATP produced. In our imaging experiments—like in most published studies, we did not distinguish whether autofluorescence arose from neurons, astrocytes or other cell types. Despite having subcellular resolution in our setups, we have no possibility to identify different cell types in our images. Unfortunately, NAD(P)H and FAD autofluorescence monitoring does not allow for measurement of absolute concentrations in the equilibrium, because of the presence of many other fluorescent molecules (e.g. porphyrins, lipoproteins and collagen; Schaefer et al., 2019; Wagnières et al., 1998).

We performed quantitative O_2 recordings at the site of autofluorescence imaging to compensate for the lacking quantification of NAD(P)H/FAD values and—more important—because the peak amplitudes only represent the net changes because of superimposed oxidative and reductive processes. However, O_2 recordings have also disadvantages since they are extracellular and punctual compared to the autofluorescence imaging of entire populations. We observed that the rates of O_2 consumption rose with stimulation frequency (Figure 3b), contrasting the decrease of autofluorescence peak amplitudes above 100 Hz (Figure 2Ca). This finding points at autofluorescence imaging being not always an appropriate measure for metabolic changes and the need for additional quantitative readouts (for discussion see Section 4.2). The relevance of O_2 consumption is given by the importance of OxPhos, which is important for ATP regeneration in MNTB neurons (Figure 3c) like in in

many neuron types (Dienel, 2019; Hall et al., 2012; Huchzermeyer et al., 2013; Ivanov et al., 2014; Ivanov & Zilberter, 2011; Özugur et al., 2020; Yellen, 2018). As we did not record APs, we do not know whether in the presence of OxPhos blockers APs were reliably elicited by each stimulus or whether the blockers induced spreading depolarization or epileptic activity as sometimes observed in the hippocampus (Kovacs et al., 2001; Malkov et al., 2014; Schuchmann et al., 2001). Therefore, we do not speculate on the quantitative contribution of OxPhos to MNTB metabolism, but only conclude that OxPhos is an important energy source for MNTB neurons.

Interestingly, the stimulation-induced O_2 changes were rather delayed and longer lasting than the stimulus period and the autofluorescence peaks (Figures 2Cb, 3a); an observation similar to the hippocampus (Foster et al., 2005; Galeffi et al., 2011) and the LSO (Brosel et al., 2018). The $t_{20/80}$ value for the O_2 drop was independent on the varying stimulus duration (except for the 40-s stimulus at 10 Hz), which is in contrast to the $t_{20/80}$ values for NAD(P)H/FAD that showed a clear correlation also for the other frequencies (Figure 2Cb). Potential causes for the slow O_2 response might be a prolonged energy demand met by OxPhos, but also diffusional aspects might have a part, because the recorded O_2 concentrations are the net result of diffusion from the medium into the slice and consumption by the cells. However, based upon our data we cannot say whether and to which extent these processes contribute to the observed alteration in O_2 concentration. We exclude that there is a principal diffusional limit to O_2-dependent reactions in our experiments, since O_2 concentrations at the minimum after stimulation were still in the range of 80 µM and the stimulated activity consumed maximal 15% of the available O_2. Also, technical limitations of the O_2 electrodes are not likely, because they have a rapid response time (90%) of 1–3 s and a detection limit of 0.3 µM.

We performed all experiments at room temperature (22.5–24.5°C), because of the longer viability of the slices at this temperature, which was crucial for applying the entire set of stimulations with 5-min breaks. In our study in the LSO, NAD(P)H/FAD peak amplitudes showed quantitative but not qualitative temperature-dependent differences (Brosel et al., 2018). We assume that temperature dependence of AP shape (Kim & von Gersdorff, 2012) and, thereby, the energy necessary for restoring ion gradients had only a small effect on our data, because we have performed all measurements at the same temperature. The non-physiological recording temperature has an impact on the overall metabolic response because of the temperature dependency of enzymes. However, Ibrahim et al. found in the hippocampus that below 29°C a tight coupling between metabolic responses and local field potential signals exists with the strongest changes in peak amplitude at 25°C (Ibrahim et al., 2017).

4.2 | Frequency dependency of metabolic responses in the MNTB

The O_2 consumption rate rose continuously with stimulation frequency up to 600 Hz and was constant above (Figure 3b). This frequency dependency is interesting for two reasons: (1) The energy demand fulfilled by OxPhos increased with frequency despite the fixed number of 400 stimuli; (2) This increase continued even above 300 Hz, when not every stimulus elicited an AP because of synaptic failures. We, thus, propose that the temporal pattern of synaptic stimulation and not only the number of pre-synaptic stimuli is determinative for the energy demand of MNTB neurons. Despite being extremely resistant to synaptic AP failures and synaptic fatigue, the MNTB is prone to electrophysiological adaptation at high stimulation frequencies (Brosel et al., 2018; Krächan et al., 2017). Synaptic plasticity like depression for long-lasting stimulation trains and accompanying changes in AP shape (e.g. broadening will definitely have an—so far unknown—effect on metabolic responses, since they affect the disturbance of ion gradients over the plasma membrane by electrical activity).

Our O_2 recordings exhibited an increase of O_2 consumption rate with stimulation frequency similar to that of NAD(P)H/FAD net peak amplitudes only up to 100 Hz, but a pronounced mismatch at higher frequencies (Figure 3d,e). Therefore, we conclude that net peak amplitudes are not under all circumstances an appropriate readout for energy demand. The cause for the lacking correlation might be found in the nature of the peak amplitudes reflecting only net changes of NAD(P)H and FAD levels by many oxidative and reductive processes, which might change their magnitude and timing with frequency. We suggest that with rising frequency energy demand increases and, therefore, the rates of both, TCA cycle and OxPhos would become larger. The rise in OxPhos rate can be deduced from the increasing rate of O_2 consumption. An even stronger increase in the rates of reductive processes might blunt the rise of net peak amplitudes as we observed for O_2 consumption rate. Another aspect to be considered is the small contribution (about 10%) of cytoplasmic NAD(P)H to the autofluorescence signal (Schaefer et al., 2019; Shuttleworth, 2010), which might have a role in the lacking correlation between NAD(P)H and O_2. This might hold especially for cellular compartments devoid of mitochondria, in which ATP is produced by glycolysis (Barros et al., 2021; Dienel, 2019; Yellen, 2018). The strong influence of the stimulus duration on the timing of the NAD(P)H/FAD peaks in contrast to O_2 consumption ($t_{20/80}$; Figure 2Cb) probably contributes to the mismatch as well.

The decreasing reliability of the MNTB synapse setting in around 300 Hz would result in not every stimulus of a train eliciting a postsynaptic action potential and, thereby, larger stimulation than firing frequencies. To consider these failures, we estimated the number of potentially elicited AP based on the well-known electrophysiology of MNTB principle neurons in in vivo and in vitro (Borst & van Hoeve, 2012; Grande & Wang, 2011; Kopp-Scheinpflug et al., 2003, 2011; Taschenberger & von Gersdorff, 2000; von Gersdorff & Borst, 2002; Wang et al., 1998). Using these estimated number of APs, we analysed the O_2 consumption rate (ΔO_2/duration) per AP and found a continuous increase over the entire frequency range (Figure 3g). This result is in accordance with our assumption that the metabolism of MNTB neurons is more dependent on the firing rate than on the total

number of elicited APs per stimulation, which we estimated to even decrease above 300 Hz (black dots in Figure 3g). However, as we did not record APs, this has to be experimentally proven.

The calyx of Held contacting MNTB principle neurons is one of a few pre-synapses, which are electrophysiological accessible. Studies showed metabolic flexibility and a changing contribution of glycolysis and OxPhos depending on firing frequency with a major contribution of OxPhos in mature animals (Lucas et al., 2018; Lujan et al., 2016, 2021). These findings support why studies in different neuron types are important, because in most neurons studied so far, calculations yielded a rather small contribution of the pre-synaptic metabolism (Howarth et al., 2012). The studies mentioned did not image NAD(P)H/FAD autofluorescence. However, we assume that a fraction of the autofluorescence signals in the MNTB originates from pre-synaptic compartments as reported for hippocampal pre-synapses (Liotta et al., 2012). This might be of relevance at stimulation frequencies above 300 Hz, when pre-synaptic electrical activity was elicited by axonal stimulation, but no post-synaptic APs were induced because of synaptic failures. We refrain from a quantitative estimation of the pre-synaptic contribution to NAD(P)H and FAD signals, because pre-synapses cannot be individually identified in our epi-fluorescence microscope.

As our data showed that the timing of synaptic stimulation is more important than the total number of stimuli, we studied how the firing pattern affects metabolic responses. Interestingly, 400 stimuli applied in bursts over a fixed 5-s-period with varying intra-burst breaks (Figure 4a–c) entailed no obvious differences to 400 stimuli continuously applied. We did not measure changes in O_2 concentration for this comparison. However, these results are in accordance with a computational study in thalamo-cortical relay neurons by Yi and Grill, who found that the metabolic demand is governed mainly by the average firing rate and not by the temporal firing pattern (Yi & Grill, 2019).

4.3 | Glucose dependency of NAD(P)H/FAD peak amplitudes

In many in vitro studies, glucose concentrations of 10 or even 25 mM were used with the aim to compensate for diffusional limitations of glucose supply (Hollnagel et al., 2020; Lourenço et al., 2019; Taschenberger & von Gersdorff, 2000). These concentrations are by far higher than the physiological value of around 2 mM, which, however, is established by a high density of blood capillaries not functional in brain slices. In our system, we found for all frequencies smaller FAD peak amplitudes for 10 mM glucose compared to those for 2 mM (Figure 4). For NAD(P)H, the differences in peak amplitudes were minute, whilst the overshoot amplitudes were much smaller for 10 mM. Despite the limitations of the NAD(P)H/FAD autofluorescence as quantitative measure (see Sections 4.1 and 4.2), we think our comparison provides some insights for electrophysiological studies, because it emphasises the importance of experimental conditions (e.g. nutrient and O_2 concentrations; Sünwoldt et al., 2017). Our data are contradictory to findings in the hippocampus, where a reduction of extracellular glucose concentration from 10 via 5 to 3 mM induced a strong decrease in NAD(P)H overshoot, whereas the NAD(P)H peak amplitude stayed constant (Ivanov et al., 2014). However, as said before, the interpretation of peak and overshoot amplitudes is difficult, because they represent net changes, and computational modelling could contribute to a better understanding. Several factors might contribute to the observed differences between the two glucose conditions, but remain to be established. This includes cytoplasmic NAD(P)H, which contributes less to cellular autofluorescence compared to mitochondrial signals (Schaefer et al., 2019; Shuttleworth, 2010), but might be especially relevant in cellular compartments without mitochondria. The impact of glucose diffusion might be different at varying extracellular glucose concentrations as well. In addition, cytoplasmic NADH could increase mitochondrial NADH and $FADH_2$ levels via the malate–aspartate shuttle (Dienel & Cruz, 2016) and the glycerol-3-P-carrier, respectively. Nevertheless, these and potential further aspects require experimental and computational validation.

5 | CONCLUSION

We found that the MNTB with its principal neurons represents a dynamic metabolic system because of its broad physiological activity range. O_2 consumption rates were by far more dependent on the frequency of pre-synaptic activity than on the number of pre-synaptic stimuli. We believe our study is relevant to other brain regions that also harbour neurons capable of high-frequency firing (Ritzau-Jost et al., 2014; Wang et al., 2016). For us, the rationale to study the metabolism of neuron types beyond the hippocampus and the cerebral cortex- is provided by the aim to further reveal the metabolic aspects of neuropathologies and improve the interpretation of functional brain imaging. Imaging of NAD(P)H and FAD autofluorescence is a simple approach to monitor metabolic responses of a large cell population with high temporal resolution and without the need of application of a sensor molecule. Nevertheless, our study showed that quantification of these signals is not always an appropriate measure and that simultaneous recording of O_2, glucose or ATP levels might be crucial. Whilst O_2 monitoring yields a quantitative readout of OxPhos, autofluorescence imaging reports the relative net balance of many metabolic processes. However, both techniques have their advantages and disadvantages. Establishing biochemical computational models will be an important step for a better understanding of the complex net changes in NAD(P)H and FAD autofluorescence signals and might reconcile the readouts of the different metabolic techniques in the future.

AUTHOR CONTRIBUTIONS

Nicola Palandt: Conceptualization; data curation; formal analysis; methodology; software; writing – original draft; writing – review and editing. **Cibell Resch:** Formal analysis; investigation; writing – review and editing. **Patricia Unterlechner:** Formal analysis; investigation;

writing – review and editing. **Lukas Voshagen:** Formal analysis; investigation; writing – review and editing. **Valentin R. Winhart:** Formal analysis; investigation; writing – review and editing. **Lars Kunz:** Conceptualization; data curation; formal analysis; funding acquisition; investigation; methodology; project administration; resources; supervision; validation; visualization; writing – original draft; writing – review and editing.

ACKNOWLEDGEMENTS

We would like to thank Benedikt Grothe for many valuable discussions and his interest in the project. For helpful comments on the project and support in the laboratory, we thank Otto Albrecht, Ian Forsythe, Cornelia Kopp-Scheinpflug, Hilde Wohlfrom and the late Hans Straka. We are grateful for financial support by the German Research Foundation (DFG; grant KU 1282/9-1). NP and VRW would like to thank the Graduate School of Systemic Neurosciences (GSN-LMU). Open Access funding enabled and organized by Projekt DEAL.

All experiments were conducted in compliance with the ARRIVE guidelines.

FUNDING INFORMATION

This study was funded by Deutsche Forschungsgemeinschaft (German Research Foundation), DFG KU 1282/9-1.

CONFLICT OF INTEREST STATEMENT

The authors have no conflict of interest to declare.

PEER REVIEW

The peer review history for this article is available at https://www.webofscience.com/api/gateway/wos/peer-review/10.1111/jnc.16091.

DATA AVAILABILITY STATEMENT

The data used and presented in this study as well as the Python script for data processing and analysis are available from the corresponding author upon reasonable request.

ORCID

Lars Kunz https://orcid.org/0000-0003-3141-0005

REFERENCES

Alle, H., Roth, A., & Geiger, J. R. P. (2009). Energy-efficient action potentials in hippocampal mossy fibers. *Science*, *325*(5946), 1405–1408. https://doi.org/10.1126/science.1174331

Barros, L. F., Ruminot, I., Martín, A. S., Lerchundi, R., Fernández-Moncada, I., & Baeza-Lehnert, F. (2021). Aerobic glycolysis in the brain: Warburg and Crabtree contra Pasteur. *Neurochemical Research*, *1*(46), 15–22. https://doi.org/10.1007/s11064-020-02964-w

Borst, J. G. G., & van Hoeve, J. S. (2012). The calyx of held synapse: From model synapse to auditory relay. *Annual Review of Physiology*, *3*(74), 199–224. https://doi.org/10.1146/annurev-physiol-020911-153236

Brennan, A. M., Connor, J. A., & Shuttleworth, C. W. (2006). NAD(P)H fluorescence transients after synaptic activity in brain slices: Predominant role of mitochondrial function. *Journal of Cerebral Blood Flow & Metabolism*, *26*(11), 1389–1406. https://doi.org/10.1038/sj.jcbfm.9600292

Brosel, S., Grothe, B., & Kunz, L. (2018). An auditory brainstem nucleus as a model system for neuronal metabolic demands. *European Journal of Neuroscience*, *47*(3), 222–235. https://doi.org/10.1111/ejn.13789

Butterfield, D. A., & Halliwell, B. (2019). Oxidative stress, dysfunctional glucose metabolism and Alzheimer Disease. *Nature Reviews Neuroscience*, *3*(20), 148–160.

Camandola, S., & Mattson, M. P. (2017). Brain metabolism in health, aging, and neurodegeneration. *The EMBO Journal*, *36*(11), 1474–1492. https://doi.org/10.15252/embj.201695810

Dienel, G. A. (2019). Brain glucose metabolism: Integration of energetics with function. *Physiological Reviews*, *99*(1), 949–1045. https://doi.org/10.1152/physrev.00062.2017

Dienel, G. A., & Cruz, N. F. (2016). Aerobic glycolysis during brain activation: Adrenergic regulation and influence of norepinephrine on astrocyte metabolism. *Journal of Neurochemistry*, *138*(1), 14–52. https://doi.org/10.1111/jnc.13630

Direnberger, S., Banchi, R., Brosel, S., Seebacher, C., Laimgruber, S., Uhl, R., Felmy, F., Straka, H., & Kunz, L. (2015). Analysis of signal processing in vestibular circuits with a novel light-emitting diodes-based Fuorescence microscope. *European Journal of Neuroscience*, *41*(10), 1332–1344. https://doi.org/10.1111/ejn.12907

Foster, K. A., Beaver, C. J., & Turner, D. A. (2005). Interaction between tissue oxygen tension and NADH imaging during synaptic stimulation and hypoxia in rat hippocampal slices. *Neuroscience*, *132*(3), 645–657.

Galeffi, F., Somjen, G. G., Foster, K. A., & Turner, D. A. (2011). Simultaneous monitoring of tissue PO2 and NADH fluorescence during synaptic stimulation and spreading depression reveals a transient dissociation between oxygen utilization and mitochondrial redox state in rat hippocampal slices. *Journal of Cerebral Blood Flow & Metabolism*, *31*(2), 626–639. https://doi.org/10.1038/jcbfm.2010.136

Grande, G., & Wang, L. Y. (2011). Morphological and functional continuum underlying heterogeneity in the spiking fidelity at the calyx of held synapse in vitro. *The Journal of Neuroscience*, *9*(31), 13386–13399. https://doi.org/10.1523/JNEUROSCI.0400-11.2011

Grothe, B., Pecka, M., & McAlpine, D. (2010). Mechanisms of sound localization in mammals. *Physiological Reviews*, *7*(90), 983–1012. https://doi.org/10.1152/physrev.00026.2009

Hall, C. N., Klein-Flugge, M. C., Howarth, C., & Attwell, D. (2012). Oxidative phosphorylation, not glycolysis, powers presynaptic and postsynaptic mechanisms underlying brain Information processing. *Journal of Neuroscience*, *6*(32), 8940–8951. https://doi.org/10.1523/JNEUROSCI.0026-12.2012

Hallermann, S., de Kock, C. P. J., Stuart, G. J., & Kole, M. H. P. (2012). State and location dependence of action potential metabolic cost in cortical pyramidal neurons. *Nature Neuroscience*, *15*, 1007–1014. https://doi.org/10.1038/nn.3132

Hollnagel, J. O., Cesetti, T., Schneider, J., Vazetdinova, A., Valiullina-Rakhmatullina, F., Lewen, A., Rozov, A., & Kann, O. (2020). Lactate attenuates synaptic transmission and affects brain rhythms featuring high energy expenditure. *iScience*, *23*(7), 101316. https://doi.org/10.1016/j.isci.2020.101316

Howarth, C., Gleeson, P., & Attwell, D. (2012). Updated energy budgets for neural computation in the neocortex and cerebellum. *Journal of Cerebral Blood Flow and Metabolism*, *32*(7), 1222–1232. https://doi.org/10.1038/jcbfm.2012.35

Huchzermeyer, C., Albus, K., Gabriel, H. J., Otáhal, J., Taubenberger, N., Heinemann, U., Kovács, R., & Kann, O. (2008). Gamma oscillations and spontaneous network activity in the hippocampus are highly sensitive to decreases in pO_2 and concomitant changes in mitochondrial redox state. *Journal of Neuroscience*, *28*(5), 1153–1162.

Huchzermeyer, C., Berndt, N., Holzhütter, H. G., & Kann, O. (2013). Oxygen consumption rates during three different neuronal activity

states in the hippocampal CA3 network. *Journal of Cerebral Blood Flow & Metabolism*, *33*(2), 263–271. https://doi.org/10.1038/jcbfm.2012.165

Ibrahim, B. A., Wang, H., Lesicko, A. M. H., Bucci, B., Paul, K., & Llano, D. A. (2017). Effect of temperature on FAD and NADH-derived signals and neurometabolic coupling in the mouse auditory and motor cortex. *Pflügers Archiv / European Journal of Physiology*, *469*(12), 1631–1649. https://doi.org/10.1007/s00424-017-2037-4

Ivanov, A., & Zilberter, Y. (2011). Critical state of energy metabolism in brain slices: The principal role of oxygen delivery and energy substrates in shaping neuronal activity. *Frontiers in Neuroenergetics*, *3*, 9. https://doi.org/10.3389/fnene.2011.00009/abstract

Ivanov, A. I., Malkov, A. E., Waseem, T., Mukhtarov, M., Buldakova, S., Gubkina, O., Zilberter, M., & Zilberter, Y. (2014). Glycolysis and oxidative phosphorylation in neurons and astrocytes during network activity in hippocampal slices. *Journal of Cerebral Blood Flow and Metabolism*, *34*(3), 397–407. https://doi.org/10.1038/jcbfm.2013.222

Karelina, K., & Weil, Z. M. (2016). Neuroenergetics of traumatic brain injury. *Concussion.*, *3*, 1. https://doi.org/10.2217/cnc.15.9

Kim, J. H., & von Gersdorff, H. (2012). Suppression of spikes during posttetanic hyperpolarization in auditory neurons: The role of temperature, I(h) currents, and the Na(+)-K(+)-ATPase pump. *Journal of Neurophysiology*, *108*(7), 1924–1932. https://doi.org/10.1152/jn.00103.2012

Koopman, W. J. H., Distelmaier, F., Smeitink, J. A. M., & Willems, P. H. G. M. (2013). OXPHOS mutations and neurodegeneration. *The EMBO Journal*, *1*(32), 9–29.

Kopp-Scheinpflug, C., Lippe, W. R., Dörrscheidt, G. J., & Rübsamen, R. (2003). The medial nucleus of the trapezoid body in the gerbil is more than a relay: Comparison of pre- and postsynaptic activity. *JARO—Journal of the Association for Research in Otolaryngology.*, *2*(4), 1–23. https://doi.org/10.1007/s10162-002-2010-5

Kopp-Scheinpflug, C., Steinert, J. R., & Forsythe, I. D. (2011). Modulation and control of synaptic transmission across the MNTB. *Hearing Research*, *279*(1), 22–31.

Kovacs, R., Schuchmann, S., Gabriel, S., Kardos, J., & Heinemann, U. (2001). Ca^{2+} Signalling and changes of mitochondrial function during low-Mg^{2+}-induced epileptiform activity in organotypic hippocampal slice cultures. *The European Journal of Neuroscience*, *13*(7), 1311–1319. https://doi.org/10.1046/j.0953-816x.2001.01505.x

Krächan, E. G., Fischer, A. U., Franke, J., & Friauf, E. (2017). Synaptic reliability and temporal precision are achieved via high quantal content and effective replenishment: Auditory brainstem versus hippocampus. *The Journal of Physiology*, *595*(3), 839–864. https://doi.org/10.1113/JP272799

Lin, M. T., & Beal, M. F. (2006). Mitochondrial dysfunction and oxidative stress in neurodegenerative diseases. *Nature*, *10*(443), 787–795.

Liotta, A., Rösner, J., Huchzermeyer, C., Wojtowicz, A., Kann, O., Schmitz, D., Heinemann, U., & Kovács, R. (2012). Energy demand of synaptic transmission at the hippocampal schaffer-collateral synapse. *Journal of Cerebral Blood Flow & Metabolism*, *32*(11), 2076–2083. https://doi.org/10.1038/jcbfm.2012.116

Lourenço, C. F., Caetano, M., Ledo, A., & Barbosa, R. M. (2019). Platinized carbon fiber-based glucose microbiosensor designed for metabolic studies in brain slices. *Bioelectrochemistry (Amsterdam, Netherlands)*, *130*, 107325. https://doi.org/10.1016/j.bioelechem.2019.06.010

Lucas, S. J., Michel, C. B., Marra, V., Smalley, J. L., Hennig, M. H., Graham, B. P., & Forsythe, I. D. (2018). Glucose and lactate as metabolic constraints on presynaptic transmission at an excitatory synapse. *The Journal of Physiology*, *596*(9), 1699–1721. https://doi.org/10.1113/JP275107

Lujan, B., Kushmerick, C., Banerjee, T. D., Dagda, R. K., & Renden, R. (2016). Glycolysis selectively shapes the presynaptic action potential waveform. *Journal of Neurophysiology*, *116*(6), 2523–2540. https://doi.org/10.1152/jn.00629.2016

Lujan, B. J., Singh, M., Singh, A., & Renden, R. B. (2021 oct). Developmental shift to mitochondrial respiration for energetic support of sustained transmission during maturation at the calyx of held. *Journal of Neurophysiology*, *126*(4), 976–996. https://doi.org/10.1152/jn.00333.2021

Malkov, A., Ivanov, A. I., Popova, I., Mukhtarov, M., Gubkina, O., Waseem, T., Bregestovski, P., & Zilberter, Y. (2014). Reactive oxygen species initiate a metabolic collapse in hippocampal slices: Potential trigger of cortical spreading depression. *Journal of Cerebral Blood Flow and Metabolism*, *34*(9), 1540–1549. https://doi.org/10.1038/jcbfm.2014.121

Mink, J. W., Blumenschine, R. J., & Adams, D. B. (1981). Ratio of central nervous system to body metabolism in vertebrates: Its constancy and functional basis. *American Journal of Physiology. Regulatory, Integrative and Comparative Physiology*, *241*(3), R203–R212. https://doi.org/10.1152/ajpregu.1981.241.3.R203

Özugur, S., Kunz, L., & Straka, H. (2020). Relationship between oxygen consumption and neuronal activity in a defined neural circuit. *BMC Biology*, *18*, 76. https://doi.org/10.1186/s12915-020-00811-6

R Core Team *R: A language and environment for statistical computing*. (2023). R Foundation for Statistical Computing. https://www.R-project.org

Raichle, M. E., & Mintun, M. A. (2006). Brain work and brain imaging. *Annual Review of Neuroscience*, *29*(1), 449–476. https://doi.org/10.1146/annurev.neuro.29.051605.112819

Ritzau-Jost, A., Delvendahl, I., Rings, A., Byczkowicz, N., Harada, H., Shigemoto, R., Hirrlinger, J., Eilers, J., & Hallermann, S. (2014). Ultrafast action potentials mediate kilohertz signaling at a central synapse. *Neuron*, *84*(1), 152–163.

Schaefer, P. M., Kalinina, S., Rueck, A., von Arnim, C. A. F., & von Einem, B. (2019). NADH autofluorescence—A marker on its way to boost bioenergetic research. *Cytometry, Part A*, *1*(95), 34–46. https://doi.org/10.1002/cyto.a.23597

Schon, E., & Przedborski, S. (2011). Mitochondria: The next (Neurode) generation. *Neuron*, *6*(70), 1033–1053.

Schuchmann, S., Kovacs, R., Kann, O., Heinemann, U., & Buchheim, K. (2001). Monitoring NAD(P)H autofluorescence to assess mitochondrial metabolic functions in rat hippocampal-entorhinal cortex slices. *Brain Research. Brain Research Protocols*, *7*(3), 267–276. https://doi.org/10.1016/s1385-299x(01)00080-0

Shulman, R. G., Hyder, F., & Rothman, D. L. (2014). Insights from neuroenergetics into the interpretation of functional neuroimaging: An alternative empirical model for studying the brain's support of behavior. *Journal of Cerebral Blood Flow and Metabolism*, *34*(11), 1721–1735. https://doi.org/10.1038/jcbfm.2014.145

Shuttleworth, C. W. (2010). Use of NAD(P)H and favoprotein autofluorescence transients to probe neuron and astrocyte responses to synaptic activation. *Neurochemistry International*, *56*(3), 379–386.

Sokoloff, L. (1981). Localization of functional activity in the central nervous system by measurement of glucose utilization with radioactive Deoxyglucose. *Journal of Cerebral Blood Flow & Metabolism*, *3*(1), 7–36. https://doi.org/10.1038/jcbfm.1981.4

Stovell, M. G., Mada, M. O., Helmy, A., Carpenter, T. A., Thelin, E. P., Yan, J. L., Guilfoyle, M. R., Jalloh, I., Howe, D. J., Grice, P., Mason, A., Giorgi-Coll, S., Gallagher, C. N., Murphy, M. P., Menon, D. K., Hutchinson, P. J., & Carpenter, K. L. H. (2018). The effect of succinate on brain NADH/NAD+ redox state and high energy phosphate metabolism in acute traumatic brain injury. *Scientific Reports*, *12*(8), 11140.

Sünwoldt, J., Bosche, B., Meisel, A., & Mergenthaler, P. (2017). Neuronal culture microenvironments determine preferences in bioenergetic pathway use. *Frontiers in Molecular Neuroscience*, *10*, 305. https://doi.org/10.3389/fnmol.2017.00305

Taschenberger, H., & von Gersdorff, H. (2000). Fine-tuning an auditory synapse for speed and Fidelity: Developmental changes in presynaptic waveform, EPSC kinetics, and synaptic plasticity. *The Journal of Neuroscience*, *12*(20), 9162–9173. https://doi.org/10.1523/JNEUROSCI.20-24-09162.2000

Trattner, B., Gravot, C. M., Grothe, B., & Kunz, L. (2013). Metabolic maturation of auditory neurones in the superior olivary complex. *PLoS One*, *8*(6), e67351. https://doi.org/10.1371/journal.pone.0067351

von Gersdorff, H., & Borst, J. G. G. (2002). Short-term plasticity at the calyx of held. *Nature Reviews Neuroscience*, *1*(3), 53–64.

Wagnières, G. A., Star, W. M., & Wilson, B. C. (1998). In vivo fluorescence spectroscopy and imaging for oncological applications. *Photochemistry and Photobiology*, *68*(5), 603–632.

Wang, B., Ke, W., Guang, J., Chen, G., Yin, L., Deng, S., He, Q., Liu, Y., He, T., Zheng, R., Jiang, Y., Zhang, X., Li, T., Luan, G., Lu, H. D., Zhang, M., Zhang, X., & Shu, Y. (2016). Firing frequency maxima of fast-spiking neurons in human, monkey, and mouse neocortex. *Frontiers in Cellular Neuroscience*, *10*, 10. https://doi.org/10.3389/fncel.2016.00239/full

Wang, L. Y., Gan, L., Forsythe, I. D., & Kaczmarek, L. K. (1998). Contribution of the Kv3.1 potassium channel to high-frequency firing in mouse auditory neurones. *The Journal of Physiology*, *509*(1), 183–194. https://doi.org/10.1111/j.1469-7793.1998.183bo.x

Watts, M. E., Pocock, R., & Claudianos, C. (2018). Brain energy and oxygen metabolism: Emerging role in normal function and disease. *Frontiers in Molecular Neuroscience*, *11*, 216.

Yellen, G. (2018). Fueling thought: Management of glycolysis and oxidative phosphorylation in neuronal metabolism. *Journal of Cell Biology*, *7*(217), 2235–2246.

Yi, G., & Grill, W. M. (2019). Average firing rate rather than temporal pattern determines metabolic cost of activity in Thalamo-cortical relay neurons. *Scientific Reports*, *12*(9), 6940.

Zsurka, G., & Kunz, W. S. (2015). Mitochondrial dysfunction and seizures: The neuronal energy crisis. *The Lancet Neurology*, *9*(14), 956–966.

Zuend, M., Saab, A. S., Wyss, M. T., Ferrari, K. D., Hösli, L., Looser, Z. J., Stobart, J. L., Duran, J., Guinovart, J. J., Barros, L. F., & Weber, B. (2020). Arousal-induced cortical activity triggers lactate release from astrocytes. *Nature Metabolism*, *2*, 179–191. https://doi.org/10.1038/s42255-020-0170-4

SUPPORTING INFORMATION

Additional supporting information can be found online in the Supporting Information section at the end of this article.

How to cite this article: Palandt, N., Resch, C., Unterlechner, P., Voshagen, L., Winhart, V. R., & Kunz, L. (2024). Metabolic response of auditory brainstem neurons to their broad physiological activity range. *Journal of Neurochemistry*, *168*, 663–676. https://doi.org/10.1111/jnc.16091